Available online at www.sciencedirect.com
SCIENCE DIRECT®
Polymer 45 (2004) 2321–2331
polymer
www.elsevier.com/locate/polymer

Effect of sodium montmorillonite source on nylon 6/clay nanocomposites

T.D. Fornes[a], D.L. Hunter[b], D.R. Paul[a,*]

[a]*Department of Chemical Engineering and Texas Materials Institute, The University of Texas at Austin, Austin, TX 78712, USA*
[b]*Southern Clay Products, 1212 Church St., Gonzales, TX 78629, USA*

Received 14 November 2003; received in revised form 9 January 2004; accepted 12 January 2004

Abstract

The effect of sodium montmorillonite source on the morphology and properties of nylon 6 nanocomposites was examined using equivalent experimental conditions. Sodium montmorillonite samples acquired from two well-known mines, Yamagata, Japan, and Wyoming, USA, were ion exchanged with the same alkyl ammonium chloride compound. The resulting organoclays were extruded with a high molecular weight grade of nylon 6 under the same processing conditions. Quantitative analysis of TEM photomicrographs of the two nanocomposites reveal a slightly larger average particle length and a slightly higher degree of platelet exfoliation for the Yamagata based nanocomposite than the Wyoming version, thus, translating into a higher particle aspect ratio. The stress–strain behavior of the nanocomposites appears to reflect the nanocomposite morphology, in that higher stiffness and strengths are attainable with the increased particle aspect ratio. Moreover, the trends in stiffness behavior between the two types of nanocomposites may be explained by conventional composite theory.

Keywords: Nylon 6; Nanocomposites; Montmorillonite

1. Introduction

The big issue in the formation of high performance polymer–clay nanocomposites is the ability to disperse the clay within the polymer. Over the last several years, a sizeable effort has been made in our laboratories to understand why layered silicates readily exfoliate within nylon 6 by melt processing techniques. Thus far, we have shown that exfoliation depends on processing conditions [1,2], melt rheology [3,4], and the structure of the alkyl ammonium compound used to modify the clay [5]. More recent investigations indicate that polyamide structure, e.g., repeat unit structure and perhaps end group concentration and configuration, plays some role in the formation of well-exfoliated nanocomposites [6,7].

In addition to the above factors, the structure of the layered silicate may influence nanocomposite morphology. The level and distribution of cationic exchange sites, the average size of the platelet stacks and of the individual platelets that comprise them, and the purity level of the clay are among many structural variables that may affect the extent of clay dispersion and the final particle size that is observed in polymer–clay nanocomposites. Several studies have attempted to address these kinds of issues. For example, Lan et al. [8] and Usuki et al. [9] showed that the type of layered silicate and its charge density leads to different levels of exfoliation during the formation of epoxy and nylon 6 nanocomposites, respectively, via polymerization-based techniques. Similar studies by Yano et al. [10] on polyimide nanocomposites made from the same clays described in the work of Usuki et al. [9] suggest that the inherent size of the clay platelets plays a dominant role in the degree of property improvement observed. Clearly, both the physical and chemical properties of the layered silicate are important factors that affect the morphology and properties of nanocomposites.

From a commercial standpoint, the type of layered silicate used in polymer nanocomposites must be abundant and easily refined in order to keep product cost at a reasonable level. Sodium montmorillonite appears to be a good candidate in this regard. Two important commercial sources of sodium montmorillonite are from mines located in Wyoming, USA and Yamagata, Japan. Sodium montmorillonite from the latter source has been extensively used by Toyota researchers [9,11–13] to formulate nanocomposites by in situ polymerization techniques. Transmission electron microscopy (TEM) investigations suggest that the

* Corresponding author. Tel.: +1-512-471-5392; fax: +1-512-471-0542.
E-mail address: drp@che.utexas.edu (D.R. Paul).

0032-3861/$ - see front matter © 2004 Elsevier Ltd. All rights reserved.
doi:10.1016/j.polymer.2004.01.061

nylon 6 nanocomposites made by Toyota using the Yamagata clay have platelets with higher aspect ratios than do nylon 6 nanocomposites formed by melt processing nylon 6 with organically modified montmorillonite from Wyoming [3,4,9,14,15]. It is unclear if this disparity stems from the different formation techniques used or from physical differences inherent to the two sources of sodium montmorillonite. This issue is addressed here by comparing nanocomposites derived from the two montmorillonite sources using the same nanocomposite formation technique.

The intent of this paper is to evaluate the effect of sodium montmorillonite source on the morphology and mechanical properties of nylon 6 nanocomposites formed under identical melt processing conditions. Wide angle X-ray scattering (WAXS) and TEM experiments are used to characterize the nanocomposite morphology, while standard stress–strain and impact strength analyses are used to assess mechanical property performance. In addition, experimental moduli are compared with predictions made using conventional composite theories.

2. Experimental

2.1. Materials and melt processing

Table 1 lists the materials used in this study. Two sodium montmorillonite clays, identified by the geographic location from which they were mined, i.e., Yamagata, Japan (YM) and Wyoming, USA (WY), were supplied from Kunimine Industries Co., Ltd and Southern Clay Products, respectively. The YM clay corresponds to the commercial product Kunipia-P®, which is a more purified version of Kunipia-F® which has been repeatedly used by Toyota to form nanocomposites by in situ polymerization. The WY clay corresponds to the commercial product Cloisite® Na^+. Each of these products were ion exchanged to near the stoichiometric equivalence with bis-(hydroxyethyl) methyl rapeseed ammonium chloride, designated here as $(HE)_2M_1R_1$, to form the organoclays designated as $(HE)_2M_1R_1$-YM and $(HE)_2M_1R_1$-WY. It should be noted that different values of the cation exchange capacity (CEC) have been reported for the Kunipia product; the value given here is based on technical information reported by Kunimine Industries Co., Ltd [16].

Nanocomposites were produced by melt mixing each organoclay with a high molecular weight (HMW) nylon 6 material using a twin screw extruder. Extruded pellets were dried and injection molded into standard tensile (ASTM D638) and Izod specimens (ASTM D256); further details of the melt processing steps used to form and shape these materials are given in prior publications [3–5]. The level of montmorillonite (MMT) in each extruded batch was determined by placing pre-dried pellets in a furnace at 900 °C for 45 min and weighing the residual ash [3,4]. All clay concentrations reported throughout the remainder of this paper correspond to the amount of inorganic silicate filler, i.e., MMT, rather than organoclay, since the silicate is the reinforcing component.

2.2. Characterization

Wide angle X-ray scattering experiments were conducted on organoclay powder and injection molded Izod specimens at a scan rate of 1°/min with Ni filtered Cu K_α X-ray radiation ($\lambda = 0.154$ nm) using a Scintag XDS 2000 diffractometer. Izod specimens were orientated such that the incident beam reflected off the major surface of the bar, as previously described [3,4]. The measured X-ray intensities for the $(HE)_2M_1R_1$-WY nanocomposites were found to be considerably less than measurements made on the same samples in a prior investigation [3,4]. The cause of the lower intensity was determined to be depletion of the copper target (X-ray source) over time. To account for this drop in intensity, all X-ray data were corrected to a fixed point in time corresponding to the prior investigation [3,4].

Transmission electron microscopy experiments were conducted on samples extracted from the core region of Izod specimens. Ultra thin sections approximately 50 nm in thickness were cryogenically cut in the plane comprised of the flow (FD) and normal directions (ND) of the specimen using a Reichert-Jung Ultracut E microtome. The resulting sections were placed on 300 mesh Cu grids and subsequently viewed with a JEOL 2010F microscope operating at 120 kV such that the electron beam was parallel to the transverse direction (TD) of the sample, i.e., normal to the FD–ND plane. Selected images were analyzed for the average particle length and the degree of clay dispersion. Complete details of the microtomy, microscopy, and image analysis techniques employed here are given in prior publications [3,4,17,18].

Standard tensile and impact properties of nylon 6 and its nanocomposites were determined according to ASTM D638 and ASTM D256 as previously outlined [3,4]. Property values reported here represent an average of the results for tests run on six specimens. Standard deviations were typically of the order of 4% for modulus, 1% for yield strength, and 15% for Izod impact strength. Elongation at break values tended to be more variable with standard deviations typically in the range of 5–25% of the value reported.

3. Results and discussion

3.1. Nanocomposite morphology

Fig. 1 shows WAXS scans of the $(HE)_2M_1R_1$-YM and $(HE)_2M_1R_1$-WY organoclays. The $(HE)_2M_1R_1$-YM organoclay scan exhibits a larger basal spacing ($d_{001} = 3.3$ nm) than the $(HE)_2M_1R_1$-WY organoclay ($d_{001} = 1.8$ nm); this effect is attributed, in part, to the different CEC values of the

Table 1
Materials used in this study

Material [designation used here]	Commercial designation	Comments/specifications	Supplier
Nylon 6 [HMW]	Capron® B135WP	High viscosity grade with $\bar{M}_n = 30,100$[a]	Honeywell
Nylon 6 [MMW]	Capron® B73WP	Medium viscosity grade with $\bar{M}_n = 22,500$[a]	Honeywell
Nylon 6 [LMW]	Capron® 8202	Low viscosity grade with $\bar{M}_n = 16,800$[a]	Honeywell
Sodium montmorillonite [YM]	Kunipia-P®	CEC = 107 milliequivalents/100 g clay (Clay source = Yamagata, Japan)	Kunimine Industries Co., Ltd
Sodium montmorillonite [WY]	Cloisite® Na^+	CEC = 92 milliequivalents/100 g clay (Clay source = Wyoming, USA)	Southern Clay Products
Bis(2-hydroxy-ethyl)methyl tallow ammonium chloride [$(HE)_2M_1\ R_1$][b]	Experimental	This amine salt was ion exchanged with each of the sodium montmorillonite materials to form the organoclays listed below.	Akzo Nobel
Organoclays			
$(HE)_2M_1\ R_1$-YM	NA	107 MER[c] % LOI = 38.7 wt%[c] d_{001} spacing = 3.3 nm[c]	NA
$(HE)_2M_1\ R_1$-WY	NA	95 MER[c] % LOI = 34.1 wt%[c] d_{001} spacing = 1.8 nm[c]	NA

[a] $\bar{M}_n$, in units of Daltons, was determined via intrinsic viscosity using *m*-cresol at 24.6 °C [29].

[b] The substituents on the quaternary ammonium compound used to form the organoclays are identified in the following shorthand notation: R = rapeseed, HE = 2-hydroxy-ethyl, and M = methyl. Rapeseed is a natural product composed predominantly of unsaturated C_{22} alkyl chains (45%).

[c] The milliequivalent ratio (MER) is a quantity describing the number of milliequivalents of amine salt used per 100 g of clay during the cationic exchange reaction with sodium montmorillonite. The loss on ignition (LOI) is the amount of volatiles evolved from per gram of dry organoclay when heating it to 900 °C for 45 min. The basal spacing corresponds to the characteristic Bragg reflection peak (d_{001}) obtained from a powder WAXS scan of the organoclay.

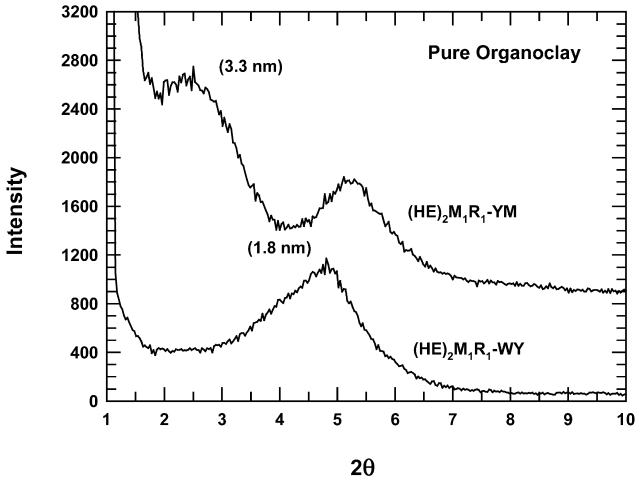

Fig. 1. WAXS scans of $(HE)_2M_1R_1$-YM and $(HE)_2M_1R_1$-WY organoclay. The $(HE)_2M_1R_1$-YM organoclay curve has been shifted for clarity.

two clays. A clay having a higher CEC will accommodate more organic modifier within its galleries and, thus, should have a higher d-spacing as found here for the YM clay. However, the observed *d*-spacing for the YM organoclay is larger than would be expected on the basis of the ratio of CEC or loss on ignition (LOI) values for the two organoclays assuming a constant density of organic material in the galleries; LOI (see Table 1) represents the mass LOI per gram of dry organoclay when heating pure organoclay at 900 °C for 45 min. Understanding this behavior would be interesting but is beyond the scope of this work

The appearance of two Bragg reflections, i.e., a primary (d_{001}) and secondary reflection (d_{002}), in the YM organoclay scan as opposed to only a primary reflection in the WY organoclay scan needs to be addressed. This effect may be explained by the height of the gallery spacing of the organoclay in relation to the thickness of a silicate platelet. Bragg reflections occur at a series of 2θ values that satisfy the Bragg equation, $n\lambda = 2d_{hkl}\sin\theta$. Also, the area under each reflection will be proportional to $\sin^2(n\pi\phi_A/2)$, where ϕ_A is the volume fraction of phase A for a two phase structure [19]. For a lamella or layered structure in which each phase shares the same cross sectional area, the volume fraction may be represented by the ratio of the thickness of phase A to the total thickness, i.e., $t_A/(t_A + t_B)$. In the situation where $t_A = t_B$, the intensity of all even ordered peaks will be reduced to zero. Since the $(HE)_2M_1R_1$-WY organoclay has a gallery height that is comparable to the thickness of a silicate platelet, such that $t_{gallery} \approx t_{platelet}$, no second order ($d_{002}$) reflection is observed.

X-ray scans for HMW nylon 6 nanocomposites made from the two types of organoclays are presented in Fig. 2. Both sets of materials exhibit smooth patterns of decreasing intensity with increasing 2θ at each MMT concentration, suggesting good dispersion of the once ordered organoclay. In addition, the level of reflected low angle X-ray scattering increases with increasing clay content which is expected when a material of high electron density is added to a

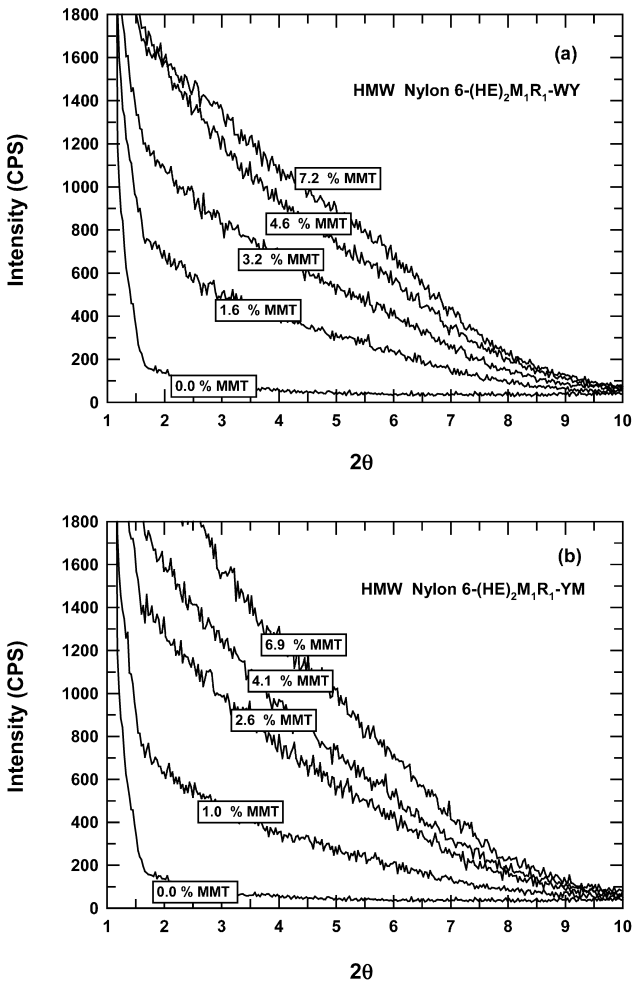

Fig. 2. The effect of MMT concentration (wt %) on the low angle scattering behavior of HMW nylon 6 nanocomposites based on (a) $(HE)_2M_1R_1$-WY and (b) $(HE)_2M_1R_1$-YM organoclay.

polymer of low electron density as repeatedly reported in the literature. Interestingly, Kojima et al. [20,21] illustrated this effect quantitatively by plotting the intensity measured at $2\theta = 4°$ versus MMT concentration for injection molded nylon 6 nanocomposites formed by in situ polymerization. They found that a linear relationship existed between the two variables. Repeating the same analysis for the present nanocomposites also reveals a direct correction between low angle scattering and MMT content (see Fig. 3); however, the slope of the $(HE)_2M_1R_1$-YM curve is higher than the $(HE)_2M_1R_1$-WY curve. This difference may be attributed to a number of effects, such as differences in platelet orientation or level of exfoliation. Previous X-ray studies conducted in this laboratory on similar nylon 6 nanocomposite materials provide some indication that scattering at low 2θ values increases with exfoliation [3,4]. Nanocomposites formed from high molecular nylon 6 materials exhibited higher degrees of clay exfoliation than those formed from a lower molecular weight (LMW) nylon 6 material (see Table 1), as verified by TEM, strain–strain, and rheological analyses, as well as WAXS experiments

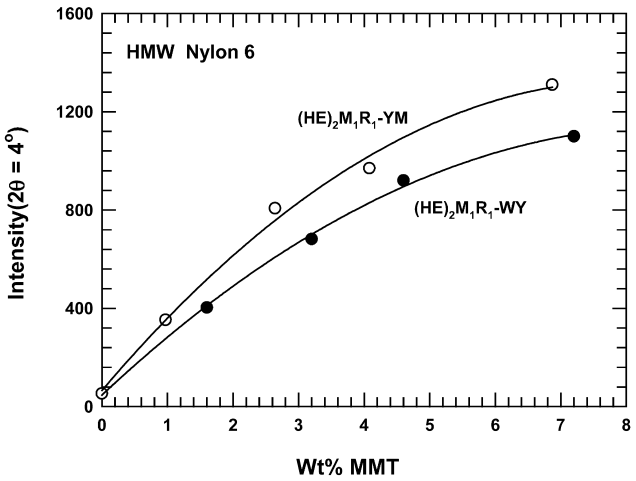

Fig. 3. The influence of the concentration and source of MMT on the reflected X-ray intensity measured at 4° of 2θ on nanocomposites based on HMW nylon 6.

[3,4]. Plotting the X-ray data for these materials in the form of intensity at $2\theta = 4°$ versus wt% MMT (see Fig. 4) shows that scattering increases with both MMT concentration and increasing level of exfoliation, i.e., the X-ray scattering from the nanocomposites based on the highest molecular weight nylon 6 is substantially greater than that from those based on the lowest molecular weight nylon 6 while the scattering from the medium molecular material is comparable to, if not slightly less than, the former (see Table 1 for description of the matrix polymers used in this comparison).

Nevertheless, the causes for the above scattering observations may be more complex in nature than simply due to exfoliation and/or orientation effects. As pointed out by Vaia and Liu [22], the intensity level obtained in reflection, especially at low 2θ values, is sensitive to a number of theoretical and experimental factors. Some important factors include polarization and interference effects, plus effects related to sample

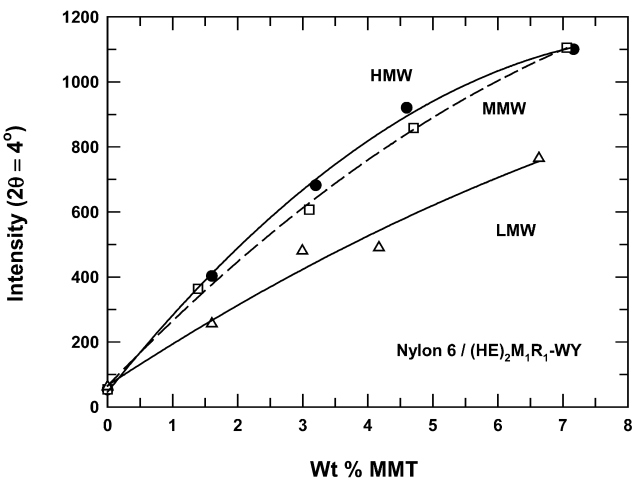

Fig. 4. The influence of MMT concentration and nylon 6 matrix molecular weight on the reflected X-ray intensity measured at $2\theta = 4°$ on nanocomposites based on $(HE)_2M_1R_1$-WY organoclay.

preparation. Effects associated with the polarization by the sample of an unpolarized beam contribute to a substantial increase in intensity with decreasing 2θ and are also sensitive to the orientation of the particles (or scatterers) within the sample. Interference effects caused by multiple scattering within and/or between particles will influence the observed intensity; in the case of nanocomposites, this will be a function of the level of exfoliation and concentration of MMT. Important factors in sample preparation consist of surface smoothness, the orientation, concentration, and distribution of particles, as well as alignment of the sample in the holder. As stressed by Vaia and Liu, careful sample preparation and data evaluation is key to interpreting X-ray data correctly. The approach taken in Figs. 3 and 4 to evaluate the present nanocomposites, although fairly simple, does minimize many of the above effects, since all samples were processed and formed into smooth injection molded parts under the same conditions and the data are analyzed at a fixed 2θ.

TEM photomicrographs of the $(HE)_2M_1R_1$-WY and $(HE)_2M_1R_1$-YM nanocomposites seen in Fig. 5 show a well-exfoliated structure consisting largely of individual clay platelets dispersed within the HMW nylon 6, which is consistent with the WAXS patterns observed earlier in Fig. 2. Also note that the platelets are highly oriented along the polymer flow direction, an observation repeatedly seen in injection molded nanocomposites [15,20,23,24]. In order to better discern between the two nanocomposite morphologies, a semi-automated image analysis procedure for measuring the degree of clay dispersion and the resulting size of clay particles was employed on a substantial number of TEM photomicrographs; in addition, the average number of platelets per clay particle was estimated by manually counting the number of platelets per particle; for explicit details of this and the aforementioned image analysis procedure the reader is referred elsewhere [17,18].

Table 2 shows the results obtained from the TEM image analysis. The number average particle length, $\bar{l}_n$, for the $(HE)_2M_1R_1$-YM nanocomposite is slightly greater than that for the WY version; histograms of the data corresponding to each average are presented in Fig. 6. Interestingly, the length of 104 nm for the $(HE)_2M_1R_1$-YM nanocomposite is in agreement with the value reported by Usuki et al. [9], i.e., $\sim$100 nm, for in situ derived nanocomposites based on nylon 6 and montmorillonite obtained from the same clay source. On the other hand, measurements by Lincoln et al. suggest that considerably higher particle lengths exist for the in situ material, i.e., 160 nm; it is unclear whether the disparity between the two reports is associated with material variations, analytical differences, e.g., microscopy techniques, TEM sample preparation, etc., or a reflection of statistical differences, such as difference in number of particles measured. If 160 nm is indeed closer to the true value, then this poses some concern of whether the shear encountered during melt

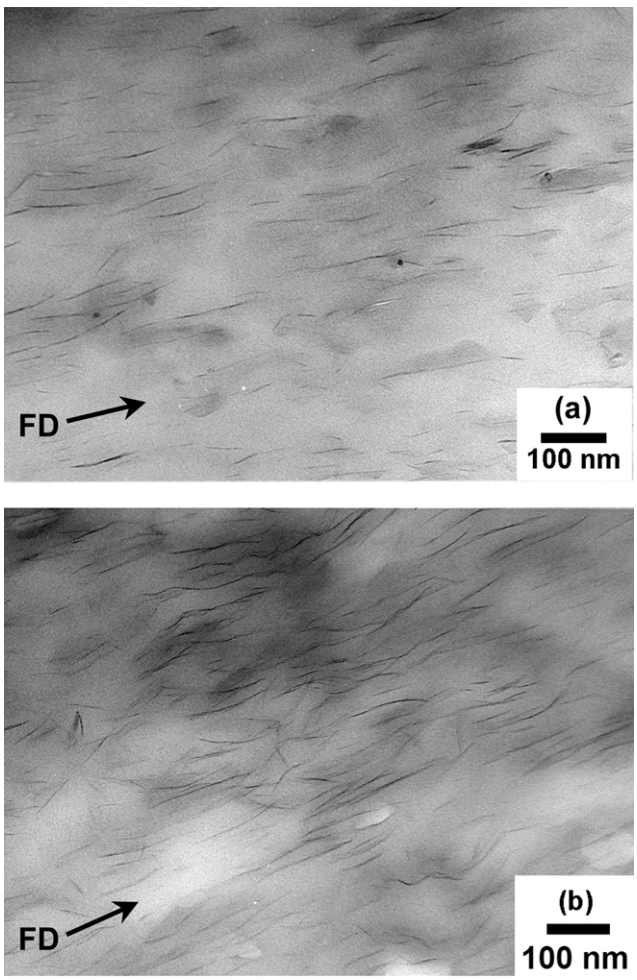

Fig. 5. TEM photomicrographs of injection molded HMW nylon 6 nanocomposites based on (a) $(HE)_2M_1R_1$-WY and (b) $(HE)_2M_1R_1$-YM organoclay.

extrusion may cause particle attrition; future studies should attempt to address this issue by characterizing platelet lengths within the organoclay prior to melt mixing with polymer.

To quantify the degree of exfoliation of each nanocomposite, the number of platelets per particle in TEM photomicrographs was estimated. Corresponding data shown in Table 2, as well as Fig. 7, suggest that degree of exfoliation is slightly larger for the $(HE)_2M_1R_1$-YM nanocomposites than the WY nanocomposite, since the average number of platelets per particles for the YM nanocomposite is less than the WY version, i.e., ~1.3 versus ~1.4, respectively. These data can be used to estimate the average particle thickness and ultimately particle aspect ratio when combined with particle length data [17]. The number average particle thickness, $\bar{t}_n$, is defined here as

$$\bar{t}_n = \frac{\Sigma(d_{001}(n-1) + t_{\text{platelet}})}{N_{\text{total}}} \quad (1)$$

where d_{001} is the repeat spacing of an unexfoliated stack of platelets, n is the number of platelets per particle, t_{platelet} is the thickness of a platelet, and N_{total} is the total number of particles. Previous investigations showed that $(HE)_2M_1R_1$-WY nanocomposites based on a low molecular weight nylon 6 material exhibited a mixed morphology of delaminated and unexfoliated platelets [3,4]. Wide angle X-ray analysis of this material revealed a broad reflection at $2\theta = 5°$, corresponding to a repeat spacing of ~1.8 nm. It is assumed that the stacks of platelets for the present $(HE)_2M_1R_1$ nanocomposites have a $d_{001} \sim 1.8$ nm. Substituting $d_{001} \sim 1.8$ nm, $t_{\text{platelet}} \sim 0.94$ nm [17], and the data shown in Fig. 7 into Eq. (1) results in a number average thickness of ~1.5 for the $(HE)_2M_1R_1$-YM nanocomposite and ~1.6 for the WY nanocomposite; this translates into a number average aspect ratio of $\bar{l}_n/\bar{t}_n = 104/1.5 = 69$ and $\bar{l}_n/\bar{t}_n = 91/1.6 = 57$, respectively. The corresponding weight average aspect ratios for the two nanocomposites are $\bar{l}_w/\bar{t}_w = 141/2.1 = 67$ and $\bar{l}_w/\bar{t}_w = 118/2.4 = 49$, respectively The larger aspect ratios for the YM nanocomposite reflects a combination of two effects, a greater platelet length and a slightly larger degree of exfoliation than the WY nanocomposites.

In addition to the average number of platelets per particle, the TEM particle density listed in Table 2 provides another indicator of degree of exfoliation; in terms of the average number of particles observed per μm^2; whereas, the specific particle density is the mean particle density normalized by filler concentration, which enables quantitative comparisons between samples having different

Table 2
Image analysis results obtained on TEM photomicrographs of injection molded HMW nylon 6 nanocomposites based on $(HE)_2M_1R_1$-WY and $(HE)_2M_1R_1$-YM organoclay

	HMW nylon 6 nanocomposite	
	$(HE)_2M_1R_1$-WY	$(HE)_2M_1R_1$-YM
MMT concentration (wt %)	3.2	2.6
Number average particle length, $\bar{l}_n$ (nm)	91	104
Weight average particle length, $\bar{l}_w$ (nm)	118	141
Number average platelets per particle	~1.4[a]	~1.3
Weight average platelets per particle	~1.7[a]	~1.5
Number average particle thickness, $\bar{t}_n$ (nm)	~1.6	~1.5
Weight average particle thickness, $\bar{t}_w$ (nm)	~2.4	~2.1
Particle aspect ratio, $\bar{l}_n/\bar{t}_n$	57	69
Particle aspect ratio, $\bar{l}_w/\bar{t}_w$	49	67
TEM particle density (μm^{-2})[b]	177	137
Specific particle density (μm^{-2})[c]	55	52

[a] Obtained in a prior TEM investigation [3].
[b] TEM particle density is the average number of particles per μm^2.
[c] Specific particle density is the TEM particle density normalized to the wt % MMT.

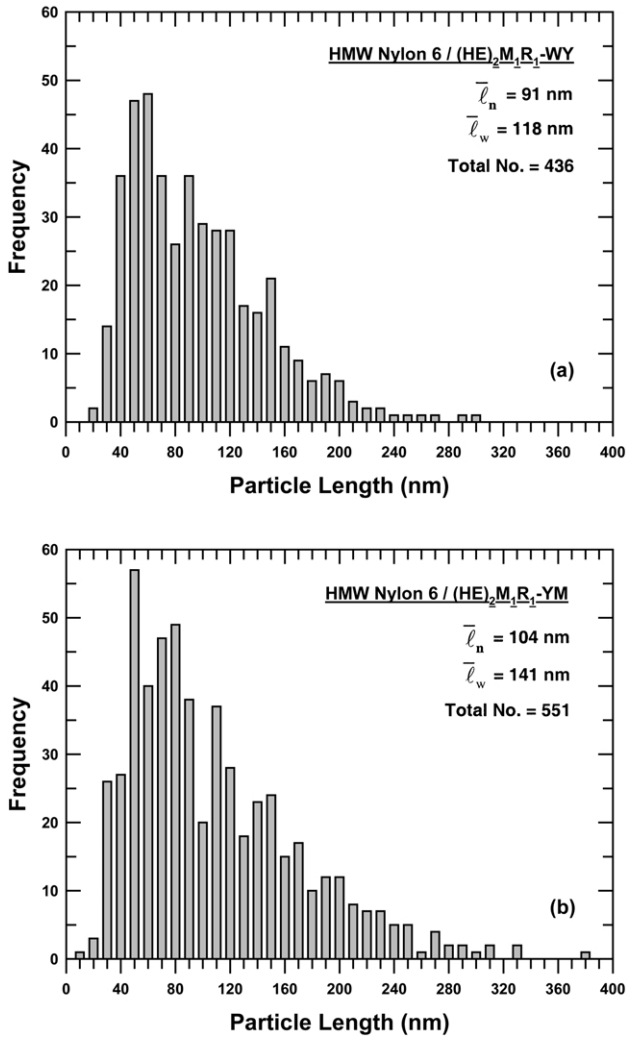

Fig. 6. Histogram of particle length data obtained by analyzing TEM photomicrographs of HMW nylon 6 nanocomposites based on (a) $(HE)_2M_1R_1$-WY and (b) $(HE)_2M_1R_1$-YM organoclay.

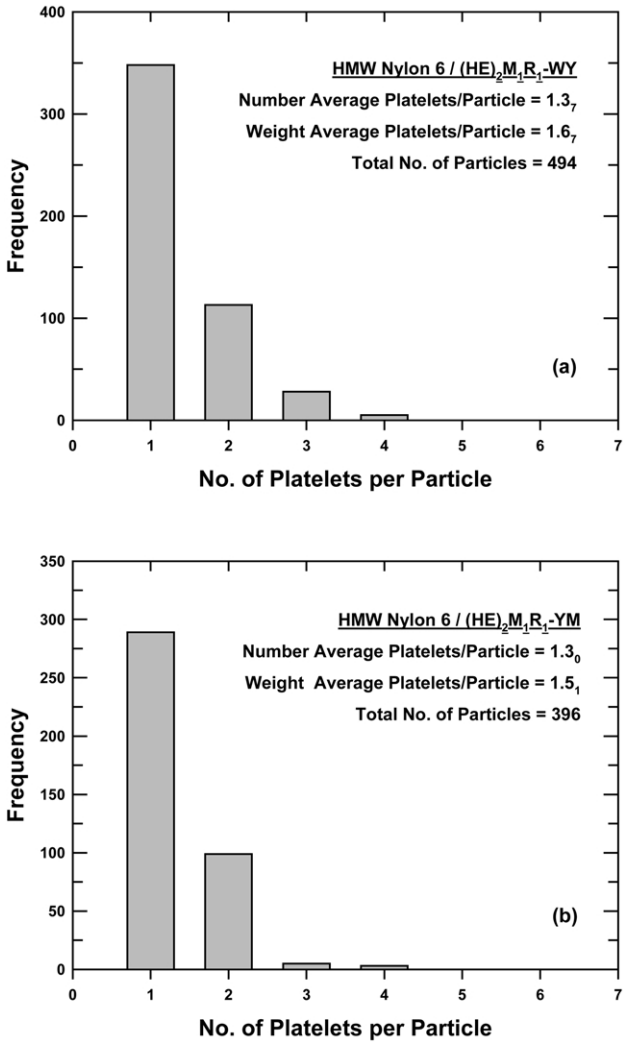

Fig. 7. Histogram of number of platelets per particle data obtained by analysis of TEM photomicrographs of HMW nylon 6 nanocomposites based on (a) $(HE)_2M_1R_1$-WY and (b) $(HE)_2M_1R_1$-YM organoclay.

amounts of MMT. The specific particle density data for the YM nanocomposite is lower than for the WY version, despite the higher degree of exfoliation as indicated by the number of platelets per particle data. The lower density primarily reflects the larger platelet length for the YM nanocomposite. For two perfectly exfoliated nanocomposites with different platelet lengths, i.e., $l_1 > l_2$, the nanocomposite with the larger platelet length, l_1, will have fewer platelets per unit volume than that of smaller platelet length when compared at a fixed weight % MMT. This may be explained quantitatively by a mass balance,

$$\text{Mass MMT/Mass Nanocomposite} = \hat{N}_1 \rho_{\text{MMT}} \pi l_1^2 t_1/4 = \hat{N}_2 \rho_{\text{MMT}} \pi l_2^2 t_2/4 \quad (2)$$

where $\hat{N}_1$ and $\hat{N}_2$ are the number of platelets per unit mass of nanocomposite, ρ_{MMT} is the density of MMT, l_1 and l_2 are the diameter of the platelets, and t_1 and t_2 represent the thickness of a MMT platelet. Note, that this equation assumes a monodisperse platelet length. If both nanocomposites are perfectly exfoliated, then Eq. (2) reduces to

$$\left(\frac{\hat{N}_2}{\hat{N}_1}\right) = \left(\frac{l_1}{l_2}\right)^2 \quad (3)$$

Therefore, for $l_1 > l_2$, $\hat{N}_2/\hat{N}_1$ will be greater than one. Substituting $l_1 \sim 104$ nm and $l_2 \sim 91$ nm in Eq. (3) results in $\hat{N}_2/\hat{N}_1 \sim 1.30$; this ratio is considerably higher than the ratio of the specific particles densities for the YM and WY nanocomposites listed in Table 2, i.e., 55/52 = 1.06, which suggests that the degree of exfoliation is less for the WY nanocomposite than the YM nanocomposite. Nevertheless, it is difficult to draw a definitive conclusion about the differences observed in specific particle density since the image analysis is compromised by the distribution of particle sizes.

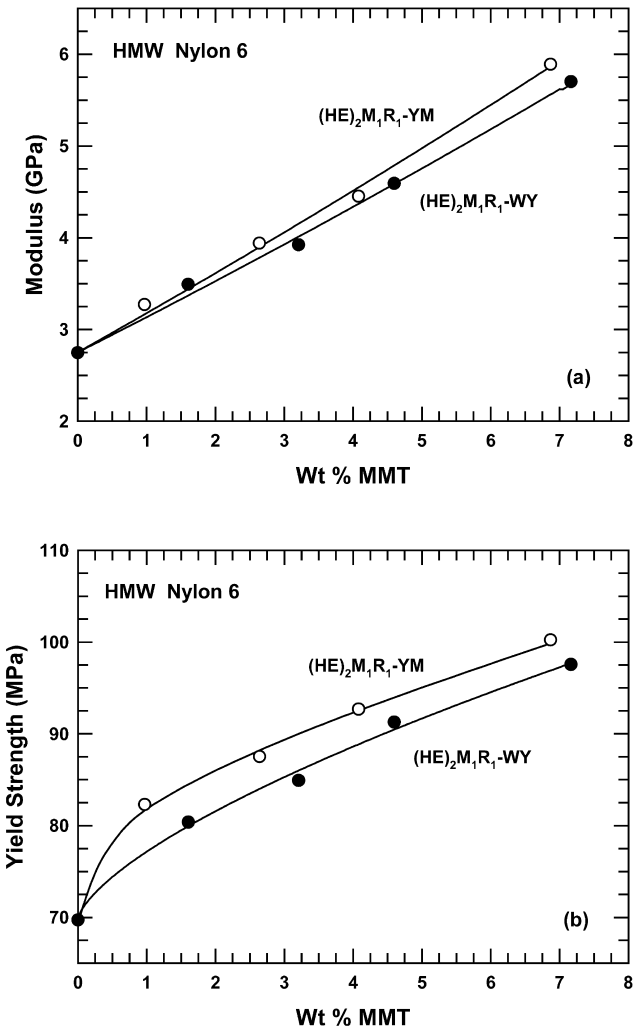

Fig. 8. The effect of the concentration and source of MMT on the (a) modulus and (b) yield strength of HMW nylon 6 nanocomposites based on $(HE)_2M_1R_1$-WY and $(HE)_2M_1R_1$-YM organoclay.

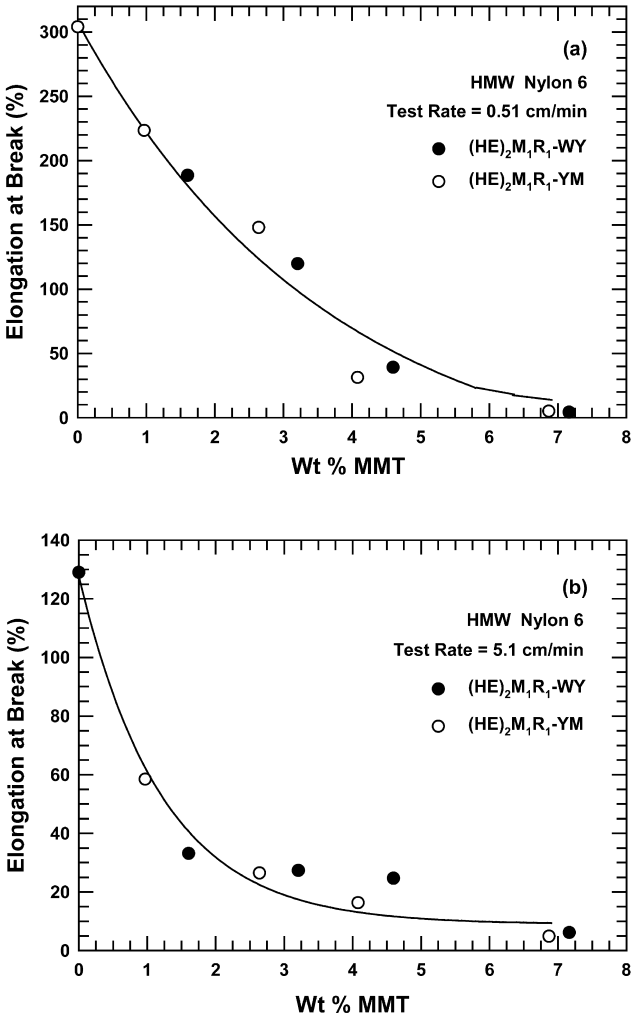

Fig. 9. The effect of the concentration and source of MMT on the elongation at break of HMW nylon 6 nanocomposites based on $(HE)_2M_1R_1$-WY and $(HE)_2M_1R_1$-YM organoclay at a crosshead speed of (a) 0.51 and (b) 5.1 cm/min.

3.2. Mechanical properties

Comparisons of the tensile properties of the two nanocomposite materials are shown in Figs. 8 and 9 (also see Table 3). Fig. 8 shows the effect of inorganic filler content (wt% MMT) on nanocomposite modulus and yield strength. Nanocomposites based on $(HE)_2M_1R_1$-YM exhibit slightly higher moduli than those based on the WY clay, particularly at high MMT concentrations (see Fig. 8(a)), while yield strengths for the $(HE)_2M_1R_1$-YM nanocomposites are consistently higher than the $(HE)_2M_1R_1$-WY nanocomposites over the MMT concentrations examined (see Fig. 8(b)). The higher level of reinforcement observed in the $(HE)_2M_1R_1$-YM nanocomposites is likely caused by higher filler aspect ratios, as indicated by the image analysis data in Table 2. The ductility of the two types of nanocomposites, as determined by elongation at break, on the other hand, is virtually the same (see Fig. 9). Increasing the clay concentration results in an equivalent sacrifice in ductility in both materials at each testing speed. Lower testing speed leads to higher elongation at break values at a given filler concentration which is to be expected.

Since the modulus of nanocomposites is well known to be highly sensitive to the degree of exfoliation, it was of interest to see if the modulus of the present and previously reported materials [3,4] correlate with the low angle X-ray scattering from these materials. Fig. 10 shows a combined plot of the data in Figs. 3 and 4. Interestingly, the nanocomposite data appear to fall on a single line regardless of the type of MMT or the nylon 6 matrix molecular weight used. The nature of this relation seems to stem from the dependency of each variable, i.e., WAXS intensity and modulus, on the degree of exfoliation.

Fig. 11 shows the relationship between Izod impact strength and MMT concentration for the two types of nanocomposites. The impact strength decreases gradually

Table 3
Mechanical properties of HMW nylon 6 nanocomposites based on $(HE)_2M_1R_1$-WY and $(HE)_2M_1R_1$-YM organoclay

Material	MMT concentration (wt%)	Modulus (GPa)	Yield strength (MPa)	Elongation at break (%)		Izod impact strength (J/m)
				Crosshead speed 0.51 cm/min	Crosshead speed 5.1 cm/min	
HMW nylon 6	0.0	2.75	69.7	304	129	44
HMW/$(HE)_2M_1R_1$-WY	1.6	3.49	80.4	189	33	43
HMW/$(HE)_2M_1R_1$-WY	3.2	3.92	84.9	119	27	45
HMW/$(HE)_2M_1R_1$-WY	4.6	4.59	91.3	39	25	45
HMW/$(HE)_2M_1R_1$-WY	7.2	5.70	97.6	4	6	46
HMW/$(HE)_2M_1R_1$-YM	1.0	3.27	82.3	223	58	36
HMW/$(HE)_2M_1R_1$-YM	2.6	3.94	87.5	148	26	36
HMW/$(HE)_2M_1R_1$-YM	4.1	4.45	92.7	31	16	34
HMW/$(HE)_2M_1R_1$-YM	6.9	5.89	100.2	5	5	33

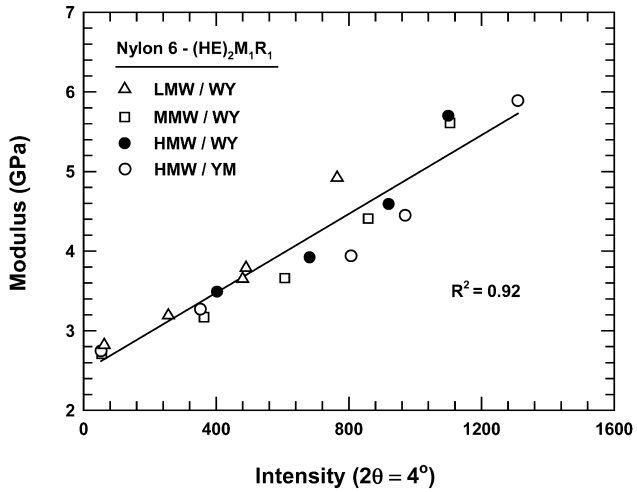

Fig. 10. Correlation between the modulus of nylon 6 nanocomposites and low angle scattering intensity taken at $2\theta = 4°$.

with increasing MMT concentration for the $(HE)_2M_1R_1$-YM nanocomposites, while the $(HE)_2M_1R_1$-WY nanocomposites are virtually independent of MMT concentration for the concentrations tested. The reasons for these observations are not entirely clear. In any case, all of these materials, including the neat nylon 6, fail in a brittle mode and the trends seen in Fig. 11 are marginally beyond normal statistical significance.

3.3. Comparison of experimental nanocomposite modulus predictions from composite theory

It was of interest to determine if the differences in stiffness of the present nylon 6 nanocomposites could be explained in terms of simple reinforcement and modeled by conventional theories of composites that assume each phase has the same properties as if the other phase were not there. Fig. 12 compares the experimental moduli for

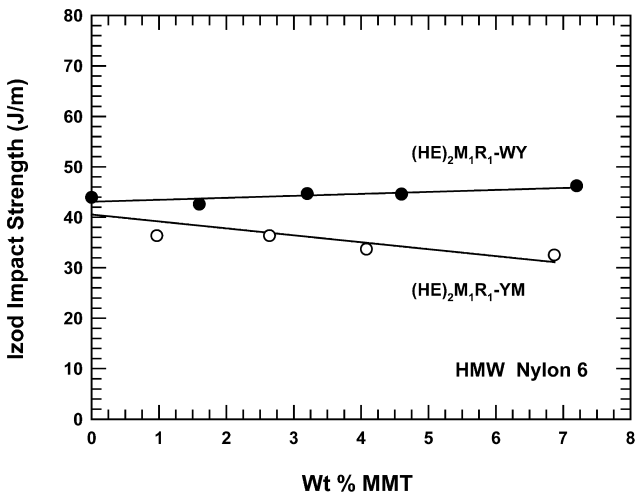

Fig. 11. The effect of the concentration and source of MMT on the Izod impact strength of HMW nylon 6 nanocomposites based on $(HE)_2M_1R_1$-WY and $(HE)_2M_1R_1$-YM organoclay.

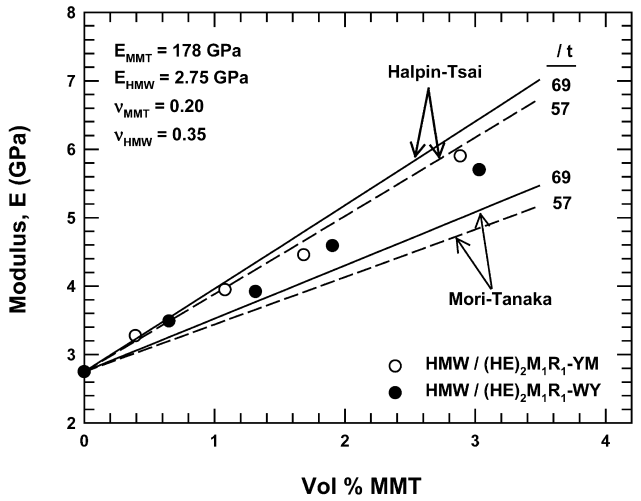

Fig. 12. Comparison of the experimentally measured modulus of the nanocomposites, E, with predictions made by the theories of Halpin–Tsai and Mori–Tanaka. The aspect ratios of $l/t = 57$ and 69 correspond to the experimentally determined number average values for HMW nylon 6 nanocomposites based on $(HE)_2M_1R_1$-WY and $(HE)_2M_1R_1$-YM organoclay, respectively. The symbols E_{MMT} and E_{HMW} represent the modulus of MMT and HMW nylon 6, respectively, whereas, ν_f and ν_m represent Poisson's ratios of MMT and HMW nylon 6, respectively. The conversion of weight % MMT to volume % MMT is based on MMT and nylon 6 densities of 2.83 and 1.14 g/cm^3, respectively.

$(HE)_2M_1R_1$-YM and $(HE)_2M_1R_1$-WY nanocomposites with predictions made by the theories of Halpin–Tsai [25,26] and Mori–Tanaka [27,28]. These two theories differ in how they approximate the filler and its effect on the composite; specific details of these two theories and their application for predicting the stiffness behavior of nanocomposites are given in a prior publication [17]. The aspect ratios of $\bar{l}_n/\bar{t}_n = 57$ and 69 used to generate the theoretical curves in Fig. 12 correspond to the experimental number average aspect ratios obtained from TEM image analysis data (Table 2) on $(HE)_2M_1R_1$-YM and $(HE)_2M_1R_1$-WY nanocomposites, respectively. In general, the theories capture the experimental stiffness trends of these nanocomposites rather well. The two theories bracket the reinforcing efficiency for the two sets of experimental data and the increase in reinforcing efficiency predicted by each theory for increasing the aspect ratio from 57 to 69 is in approximately the same proportion as the experimental values. A more quantitative illustration of the latter effect is given in Table 4 which lists the slopes of each data set and the ratio of the reinforcing efficiency for the two aspect ratios.

4. Conclusions

Nylon 6 nanocomposites based on two well-known sources of montmorillonite, Yamagata, Japan, and Wyoming, USA, were formed by twin screw extrusion. Detailed morphological studies on the two types of nanocomposites indicate that the Yamagata clay is comprised of platelets that are slightly larger than those of the Wyoming clay. The larger particle lengths, in addition to a slightly higher degree of platelet exfoliation, observed for nanocomposites made from the Yamagata clay translates into a higher particle aspect ratio than observed for nanocomposites made from the Wyoming clay. Trends in tensile properties appear to reflect the nanocomposite structure in that higher stiffness and strengths are obtained for the Yamagata nanocomposite per unit mass of montmorillonite. Moreover, the difference in stiffness behavior caused filler aspect ratio is adequately explained by conventional composite theory. Future studies should determine whether platelet attrition occurs during melt processing.

Table 4
Comparison between theoretical and experimental reinforcing efficiency for nylon 6/clay nanocomposites

Aspect ratio ($\bar{l}_n/\bar{t}_n$)	Reinforcing efficiency = dE/d(vol% MMT)		
	Halpin–Tsai	Mori–Tanaka	Experimental
57	1.13	0.69	0.96[a]
69	1.21	0.78	1.06[b]
Ratio	1.07	1.12	1.11

[a] Based on $(HE)_2M_1R_1$-WY experimental data.
[b] Based on $(HE)_2M_1R_1$-YM experimental data.

Acknowledgements

This work was supported by the Air Force Office of Scientific Research. Special thanks are given to Mr Randy Chapman of Southern Clay products for assistance with WAXS measurements.

References

[1] Cho JW, Paul DR. Polymer 2001;42(3):1083–94.
[2] Dennis HR, Hunter DL, Chang D, Kim S, White JL, Cho JW, Paul DR. Polymer 2001;42(23):9513–22.
[3] Fornes TD, Yoon PJ, Keskkula H, Paul DR. Polymer 2001;42(25):9929–40.
[4] Fornes TD, Yoon PJ, Keskkula H, Paul DR. Polymer 2002;43(7):2121–2.
[5] Fornes TD, Yoon PJ, Hunter DL, Keskkula H, Paul DR. Polymer 2002;43(22):5915–33.
[6] Fornes TD, Paul DR. In preparation.
[7] Chavarria F, Paul DR. In preparation.
[8] Lan T, Kaviratna PD, Pinnavaia TJ. Chem Mater 1995;7(11):2144–50.
[9] Usuki A, Koiwai A, Kojima Y, Kawasumi M, Okada A, Kurauchi T, Kamigaito O. J Appl Polym Sci 1995;55(1):119–23.
[10] Yano K, Usuki A, Okada AJ. J Polym Sci, Part A: Polym Chem 1997;35(11):2289–94.
[11] Okada A, Fukushima Y, Kawasumi M, Inagaki S, Usuk A, Sugiyami S, Kurauchi T, Kamigaito O. United States, Patent No. 4739007, 1988 (assigned to Toyota Motor Co., Japan).
[12] Usuki A, Kojima Y, Kawasumi M, Okada A, Fukushima Y, Kurauchi T, Kamigaito O. J Mater Res 1993;8(5):1179–84.

[13] Okada A, Usuki A. Mater Sci Engng 1995;C3:109–15.
[14] Lincoln DM, Vaia RA, Wang Z-G, Hsiao BS. Polymer 2001;42(4): 1621–31.
[15] Yoon PJ, Fornes TD, Paul DR. Polymer 2002;43(25):6727–41.
[16] Suzuki K. Plastics (Japan) 2000;51(9):81–5.
[17] Fornes TD, Paul DR. Polymer 2003;44(17):4993–5013.
[18] Fornes TD. Polyamide-layered silicate nanocomposites by melt processing, PhD Dissertation. The University of Texas at Austin, Chem Engng 2003.
[19] Roe RJ. Methods of x-ray and neutron scattering in polymer science. New York: Oxford University Press; 2000. p. 194–6.
[20] Kojima Y, Usuki A, Kawasumi M, Okada A, Kurauchi T, Kamigaito O, Kaji KJ. J Polym Sci, Part B: Polym Phys 1994; 32(4):625–30.
[21] Kojima Y, Usuki A, Kawasumi M, Okada A, Kurauchi T, Kamigaito O, Kaji KJ. J Polym Sci, Part B: Polym Phys 1995;33(7):1039–45.
[22] Vaia RA, Liu W. J Polym Sci, Part B: Polym Phys 2002;40(15): 1590–600.
[23] Akkapeddi MK. Annu Tech Conf—Soc Plast Engng 1999;2(57): 1619–22.
[24] Masenelli-Varlot K, Reynaud E, Vigier G, Varlet J. J Polym Sci, Part B: Polym Phys 2001;40(3):272–83.
[25] Halpin JC, Kardos JL. Polym Engng Sci 1976;16(5):344–52.
[26] Halpin JC, Finlayson KM, Ashton JE. Primer on composite materials analysis, 2nd ed. Lancaster, PA: Technomic; 1992.
[27] Mori T, Tanaka K. Acta Metall 1973;21:571–4.
[28] Tandon GP, Weng GJ. Polym Comp 1984;5(4):327–33.
[29] Fornes TD, Yoon PJ, Paul DR. Polymer 2003;44(24):7545–56.